Transactions in GIS

WILEY

Transactions in GIS

RESEARCH ARTICLE OPEN ACCESS

Detecting *Pteridium arachnoideum* and *Tithonia diversifolia* in a Multiclass Land-Cover Framework in the Cerrado: A Deep Learning Time-Series Benchmark With Spatial Cross-Validation

Leandro de Arruda Bruno[1] | Osmar Abílio de Carvalho Júnior[1] | Osmar Luiz Ferreira de Carvalho[2] | Potira Meirelles Hermuche[1]

[1]Department of Geography, University of Brasília, Brasília, Brazil | [2]Department of Electrical Engineering, University of Brasília, Brasília, Brazil

Correspondence: Osmar Abílio de Carvalho Júnior (osmarjr@unb.br)

Received: 8 October 2025 | **Revised:** 15 February 2026 | **Accepted:** 9 March 2026

Keywords: Cerrado biome | deep learning | encroaching species | NICFI time series | remote sensing | spatial cross-validation

ABSTRACT

This study presents the first deep-learning time-series benchmark for detecting two encroaching species in the Brazilian Cerrado: the native super-dominant fern *Pteridium arachnoideum* and the invasive alien shrub *Tithonia diversifolia*. We evaluate 43 architectures across six families (CNNs, RNNs, Transformers, and three hybrid groups) on monthly Planet NICFI satellite imagery in Brazil's Federal District, adopting a 13-class land-use/land-cover scheme with 16,250 samples. CNNs and hybrid CNN + RNN models achieve the highest accuracy, with FCN and LSTM-FCN emerging as the most robust architectures (F1 > 98% under random splitting, ~82% under spatial cross-validation). *Tithonia diversifolia* is reliably detected across spatially independent regions owing to its distinctive flowering phenology (F1 > 95%), whereas *P. arachnoideum* exhibits greater spatial variability (F1 > 76%) due to spectral overlap with forest formations. Wall-to-wall classification maps confirm ecologically coherent spatial distributions for both species. Spatially independent five-fold cross-validation reveals that conventional random splitting inflates performance by 16–25 percentage points across all architecture groups. These results provide practical guidance for selecting architectures suited to operational monitoring and underscore the importance of spatially independent evaluation in remote-sensing classification.

1 | Introduction

The spread of encroaching species is a major international challenge recognized by the Convention on Biological Diversity (Maney et al. 2024). Intensified by global connectivity and population growth (Pyšek et al. 2020; Xu et al. 2022), it leads to biotic homogenization, biodiversity loss, altered fire regimes, and the decline of native species (Mandle et al. 2011; Sampaio and Schmidt 2014).

In the Cerrado biome, two species stand out as particularly problematic: the native fern *Pteridium arachnoideum* (syn. *Pteridium aquilinum var. arachnoideum*) and the exotic shrub *Tithonia diversifolia* (Mexican sunflower). *Pteridium arachnoideum* is a native fern that has become super-dominant in degraded Cerrado areas, forming dense monodominant stands that suppress native vegetation recovery (Guerin and Durigan 2015). While some earlier studies used the term "invasive" to describe its aggressive spread, recent ecological frameworks (IPBES 2023; Soto et al. 2024) distinguish between alien invasive species and native species that exhibit opportunistic expansion following anthropogenic disturbance. Accordingly, we characterize *P. arachnoideum* as a native super-dominant species (Pivello et al. 2018) whose

This is an open access article under the terms of the Creative Commons Attribution License, which permits use, distribution and reproduction in any medium, provided the original work is properly cited.

© 2026 The Author(s). *Transactions in GIS* published by John Wiley & Sons Ltd.

proliferation is primarily driven by land-use change, fire regime alteration, and habitat degradation, rather than by inherent invasive traits. This species spreads through sexual reproduction and underground rhizomes that confer resistance to cutting, herbicides, and fire (Marrs and Watt 2006), while its dense fronds intercept sunlight before it reaches the soil, suppressing the growth of other plants, and its allelopathic properties further inhibit the establishment of competing species (Taylor and Thomson 1990; Marrs and Watt 2006).

Tithonia diversifolia (Mexican sunflower) is an invasive alien shrub native to Central America, characterized by rapid growth and the ability to propagate both by seed and vegetatively (Tongma et al. 2001; Muoghalu and Chuba 2005; Ajao and Moteetee 2017). It competes with native species through allelopathic effects that inhibit germination and growth, and is widely found in degraded areas, roadsides, and vacant lots. Officially listed as invasive in the Federal District (Instituto Brasília Ambiental—IBRAM 2021), its bright yellow flowering between April and June facilitates field identification. However, few studies have addressed its spatial mapping; a notable exception is Tuyizere et al. (2018), who used geographic information systems and spatial extrapolation techniques.

Early detection and monitoring of encroaching species are crucial for mitigating their ecological impacts (Cook et al. 2007). Remote sensing has become key for this purpose, particularly as advances in orbital and aerial (drone) sensors improve spatial, spectral, and temporal resolution (Huang and Asner 2009; Mouta et al. 2021). Several reviews discuss remote sensing applications for invasive plant detection (He et al. 2011; Bradley 2014; Rocchini et al. 2015; Ismail et al. 2016; Niphadkar and Nagendra 2016; Vaz et al. 2018; Royimani et al. 2019; Ahmed et al. 2020; Villalobos Perna et al. 2023; Zaka and Samat 2024; Singh et al. 2024). Remotely detectable features of target species include spectral changes linked to allelopathy (Liu et al. 2006; Kalisz et al. 2021), habitat structure modification (Asner et al. 2008; Große-Stoltenberg et al. 2025), fire adaptation (Berry et al. 2011; Nunes et al. 2020), climate-driven range shifts (Beaury et al. 2020; Turbelin and Catford 2021), and plant community alteration (Lazzaro et al. 2020).

Two remote sensing approaches have proven particularly relevant: (a) time-series analysis, which captures phenological dynamics, and (b) deep learning (DL) methods, which enhance detection accuracy. While some studies rely on single scenes focused on phenological extremes (e.g., flowering or senescence) (Somodi et al. 2012), time series provide a more complete picture of seasonal variation and improve separability between target and native species (Evangelista et al. 2009). DL has substantially advanced remote sensing, particularly for land cover and agricultural mapping (Wang et al. 2022). However, recent reviews on invasive plant detection (Rakgoale and Ngetar 2024; Zaka and Samat 2024) highlight that most studies still rely on conventional methods. The application of DL to satellite image time series classification has been growing rapidly (Ismail Fawaz et al. 2019; Simões et al. 2021), enabling automatic feature extraction from raw spectral-temporal sequences, non-linear temporal dependency modeling, and scalability to large datasets. At the same time, the combined use of DL architectures with time series for target plant detection remains largely unexplored in terrestrial ecosystems. Representative studies include applications to *Spartina alterniflora* (Tian et al. 2020; Min et al. 2025; Chen et al. 2020), leafy spurge (*Euphorbia virgata*/*E. esula*) (Lake et al. 2022), water lettuce (*Pistia stratiotes*) (Hao et al. 2024), cheatgrass (*Bromus tectorum*) (Larson and Tuor 2021), and *Pedicularis kansuensis* (Zhu et al. 2025). These studies have demonstrated promising results, particularly in aquatic and coastal ecosystems; however, applications in heterogeneous terrestrial environments remain scarce.

This research aims to detect the target plants *P. arachnoideum* and *T. diversifolia* in the Cerrado biome using DL time-series classifiers applied to monthly Planet NICFI composite imagery. To date, neither species has been mapped using time-series DL approaches. Specifically, the study pursues four objectives: (a) explore the underused Planet NICFI data for target-plant detection in the Cerrado, (b) compare 43 DL architectures organized into six groups (CNNs, RNNs, Transformers, Hybrid Transformer + RNN, Hybrid Transformer+CNN, and Hybrid CNN + RNN) in a multiclass setting with 13 LULC classes, (c) quantify the effect of spatial autocorrelation on apparent model performance by contrasting random and spatially independent evaluation strategies, and (d) assess per-species detectability across spatially independent regions.

2 | Material and Methods

The methodology consisted of the following steps: (a) acquisition of the Planet NICFI image time series and creation of monthly mosaics; (b) construction of the spatiotemporal cube; (c) analysis of the phenological behavior of natural vegetation and target plants and sample collection for training and validation; (d) experimental design; (e) comparison of classification methods, including training protocol and computational setup; (f) accuracy analysis; and (g) spatial analysis (Figure 1).

2.1 | Study Area

The Federal District is located in the central region of Brazil, in the Central Plateau (Centre-West region), near the confluence of the Amazon, Tocantins-Araguaia, and São Francisco River basins. The climate has two distinct seasons: the rainy season (October to April) and the dry season (May to September). The region has varied relief, with altitudes ranging from 850 to 1340 m, including flat areas, gentle undulations, and dissected terrain along the main rivers. The Cerrado, the predominant biome in the area, is a mosaic of vegetation, divided into three main categories: forest, savanna, and grassland (Ribeiro and Walter 1998).

The Cerrado, recognized as the most biodiverse savanna in the world, is home to 12,385 catalogued native plant species, of which approximately 4000 are endemic to the region. However, it is estimated that 40% of its original vegetation has already been lost, reaching almost 60% in the Federal District. The Cerrado biome is considered one of the 25 global biodiversity hotspots, characterized by high biological diversity, a high degree of endemism, and a serious threat to its conservation (Myers et al. 2000).

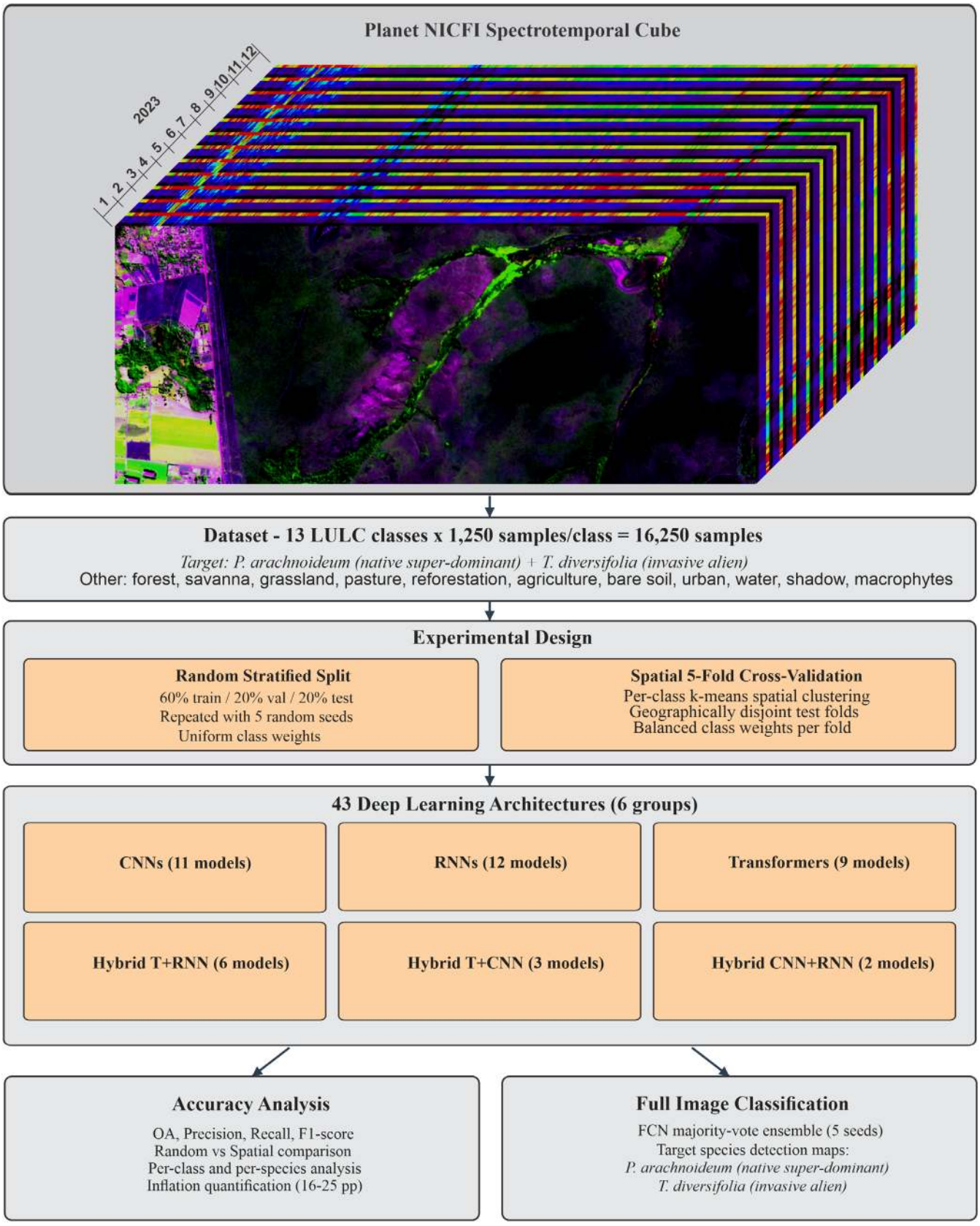


FIGURE 1 | Methodological flowchart. Monthly Planet NICFI composites (January–December 2023; 4 bands, 4.77 m) are stacked into a spectrotemporal cube and sampled across 13 LULC classes (16,250 points). Two evaluation strategies are applied: Random stratified split (5 seeds) and spatial five-fold cross-validation with geographically disjoint regions. Forty-three deep learning architectures, organized into six groups, are benchmarked under both strategies. Outputs include accuracy analyses (random vs. spatial comparisons) and wall-to-wall classification maps for target species detection.

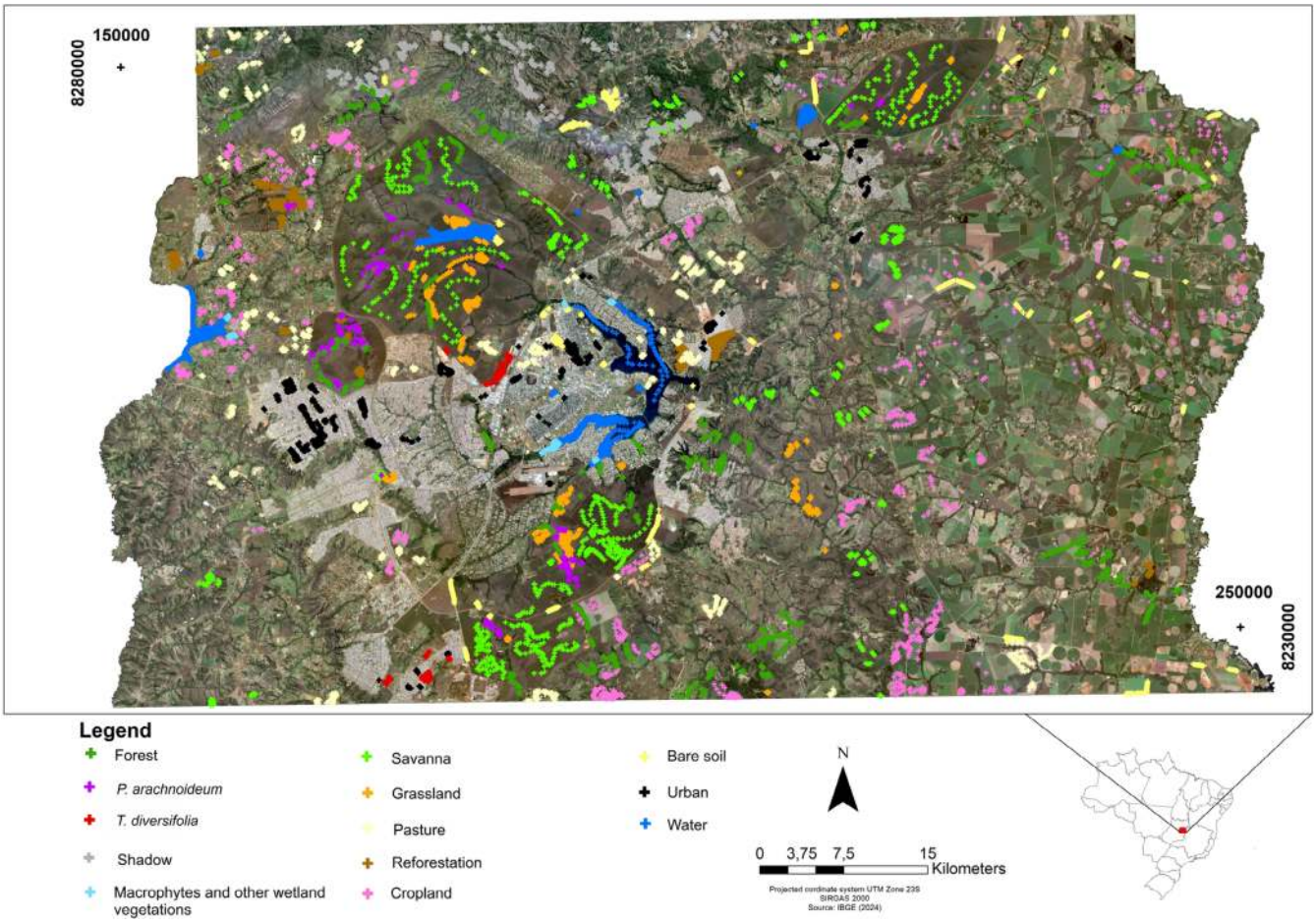


FIGURE 2 | Sampling points used for training and validation across Brazil's Federal District, colored by class (see legend): Forest, savanna, grassland, pasture, reforestation, cropland, bare soil, urban, water, shadow, macrophytes and other wetland vegetations, and the two target species *P. arachnoideum* and *T. diversifolia*. Points are overlaid on a satellite RGB basemap; the inset locates the Federal District within Brazil. Coordinates in SIRGAS 2000/UTM Zone 23S.

Although it shares some species with adjacent biomes, the Cerrado flora is highly distinctive, with a large proportion of endemic taxa.

2.2 | Image Acquisition

NICFI released 4.77-m resolution mosaics from the Planet satellite, covering an area of 45 million square kilometers (NICFI 2024). The images are from the Dove satellite constellation, a low-orbit, daily-revisit satellite with four spectral bands: blue (455–515 nm), green (500–590 nm), red (590–670 nm), and near-infrared (780–860 nm) (Planet Team 2024). NICFI data from 2015 to 2020 consist of composite images accumulated over 3–6 months. Beginning in September 2020, mosaics with individual monthly composites became available. The time series comprises 12 monthly composite images (January–December 2023) from the Planet NICFI programme, with one cloud-free mosaic per month ($N = 12$ time steps). The NICFI mosaics are generated as monthly best-pixel composites that minimize cloud contamination; therefore, the delivered products are nominally cloud-free. Each Planet NICFI tile corresponds to 20×20 km of ground and has 4096×4096 pixels. For the Federal District, we used the 12 monthly composites from 2023 and stacked them in ArcGIS to build the temporal cube.

2.3 | Dataset

The sample selection followed a stratified sampling design based on 13 land-use and land-cover (LULC) classes, including the two target species (*P. arachnoideum* and *T. diversifolia*) and 11 additional targets: water bodies, forest formations, grassland formations, savanna formations, pastures, reforestation areas, agricultural areas, exposed soil, urban areas, shade, and macrophytes and other wetland vegetation (Figure 2). This design aimed to represent the environmental heterogeneity of the study area and to reduce potential spectro-temporal confusion with the target species. An equal number of samples per class ($n = 1250$) was collected to ensure class balance during model training (Foody 2002; Estabrooks et al. 2004), totaling 16,250 samples (Figure 2). Within each stratum, samples were spatially distributed across different portions of the study area to ensure representativeness and to avoid excessive clustering. An initial reconnaissance field survey identified representative infestation patches and

characterized their morphological and phenological patterns. Based on this reconnaissance, candidate samples for both target species and other LULC classes were selected through visual interpretation of high-resolution imagery (Google Earth and Planet NICFI mosaics). A subsequent field campaign verified the selected locations and confirmed class attribution in situ. Each sample was defined as a single 4.77 m pixel on the imagery and subsequently verified in the field.

The identification of target species in situ was not ambiguous due to their distinctive morphological and phenological characteristics. The main infestation areas are well established by the management agencies of conservation units in the Federal District, including Brasília National Park and Brasília National Forest (managed by ICMBio), the IBGE Ecological Reserve (managed by IBGE), and Boca da Mata Ecological Park (managed by IBRAM). High-resolution imagery from Google Earth was used as auxiliary support for delineating infestation patches, particularly in extensive or difficult-to-access areas. Transitional environments and structurally similar vegetation posed local challenges; these were mitigated by applying a dominance criterion within the pixel footprint and by modeling multiple LULC classes to account for potential confusion.

2.4 | Experimental Design

The 16,250 samples were partitioned into training, validation, and test subsets under two complementary evaluation strategies, applied identically to all 43 DL architectures, to quantify the effect of spatial autocorrelation on apparent model performance.

- *Random stratified split*. Each run randomly assigned 60% of the samples to training (9750), 20% to validation (3250), and 20% to test (3250), preserving class proportions via stratification. This procedure was repeated with five random seeds [42, 123, 456, 789, 1024], providing a baseline that includes spatial autocorrelation effects, consistent with common practice in the literature.
- *Stratified spatial fivefold cross-validation*. Sample coordinates were grouped into five geographically disjoint regions through a per-class spatial clustering procedure: k-means ($k = 5$) was applied independently to the geographic coordinates of each LULC class, producing five spatially coherent groups per class, and samples sharing the same cluster index across all 13 classes were then pooled into a single fold (Figures S1 and S2). This per-class approach ensures that every fold contains representatives of all classes; a joint clustering over all samples would risk concentrating less frequent classes in one or two folds. The number of folds was set to five as a trade-off between spatial separation and sample adequacy: fewer folds would yield larger spatial blocks but reduce the number of independent test iterations, whereas more folds would shrink the geographic extent of each block and weaken the intended disruption of spatial autocorrelation. Given the relatively large dataset (16,250 samples distributed across 13 classes), five folds ensure sufficiently large test sets while preserving geographic separation, producing test sets averaging ~3250 samples (~250 per class), which is sufficient for stable metric estimation. The choice of five folds is grounded in the bias–variance trade-off that governs cross-validation design, where $k = 5$ or $k = 10$ has been shown to yield reliable accuracy estimates without excessive computational cost (Kohavi 1995; Valavi et al. 2019), while also satisfying the spatial validation requirement of geographically separated folds for realistic performance assessment (Roberts et al. 2017; Ploton et al. 2020). In each iteration, one region served as the test set, and the remaining four were split randomly (75/25) into training and validation subsets. A random rather than spatial partition was adopted at this stage because the validation subset serves solely for checkpoint selection (lowest validation loss) and does not contribute to the reported performance metrics, which derive entirely from the spatially independent test fold. An additional spatial split would reduce the effective training pool at each iteration, risking unstable convergence for the deeper architectures evaluated. Because the spatial regions differ in extent, fold sizes are unequal: test sets range from 1976 to 4588 samples (mean 3250), with corresponding training sets of 8746–10,705 and validation sets of 2916–3569. Class weights inversely proportional to training-fold class frequencies were applied to address the per-fold class imbalance introduced by spatial partitioning.

By comparing results from both strategies, we directly quantify the degree to which spatial autocorrelation inflates performance estimates. For each class, counts of true positives (TP), true negatives (TN), false positives (FP), and false negatives (FN) were derived, and four complementary metrics were reported: Overall Accuracy (OA), macro-averaged Precision (P), Recall (R), and F1-score.

2.5 | DL Architectures for Time Series Classification

This study evaluated all 43 time-series classification architectures available in the *tsai* library (Oguiza 2023), organized into six groups: pure CNNs (11 models), pure RNNs (12), Transformers (9), Hybrid Transformer+RNN (6), Hybrid Transformer+CNN (3), and Hybrid CNN + RNN (2). For several architectures, the library provides "Plus" variants that incorporate additional regularization, normalization, and dropout layers to improve training stability. The benchmark model choice is supported by the dataset size (16,250 samples), which favors DL over conventional classifiers.

CNN-based methods apply one-dimensional convolutions to extract temporal patterns at multiple scales. The Fully Convolutional Network (FCN) (Wang et al. 2017) uses three convolutional blocks followed by global average pooling, offering a lightweight yet effective baseline. The Residual Network (ResNet) (He et al. 2016) adds shortcut connections that mitigate gradient degradation in deeper networks. InceptionTime (Ismail Fawaz et al. 2020) applies parallel filters of varying kernel sizes within each module, capturing patterns at multiple temporal resolutions

simultaneously. The Temporal Convolutional Network (TCN) (Lea et al. 2017; Bai et al. 2018) employs dilated causal convolutions to expand the receptive field exponentially while preserving temporal ordering. The Explainable Convolutional Network (XCM) (Fauvel et al. 2021) applies separate convolutions to each input variable before combining them, enabling variable-level attribution. OmniScale CNN (Tang et al. 2022) generates features across all possible temporal scales through a parameterised scale-selection mechanism, and Xception-Time (Rahimian et al. 2020) uses depthwise separable convolutions for efficient multi-scale feature extraction.

RNNs model sequential dependencies through recurrent cells. We evaluated Long Short-Term Memory (LSTM) (Hochreiter and Schmidhuber 1997), which uses gating mechanisms to selectively retain or forget information across time steps, and Gated Recurrent Unit (GRU) (Cho et al. 2014), a simplified variant with fewer parameters. Their bidirectional variants, Bi-LSTM (Graves and Schmidhuber 2005) and Bi-GRU (Luo et al. 2018), process the sequence in both directions to capture past and future context. Attention-based versions (Bahdanau et al. 2015; Luong et al. 2015) assign learned weights to individual time steps, allowing the model to focus on phenologically discriminative periods within the series.

Transformer methods (Vaswani et al. 2017) exploit self-attention to capture long-range dependencies in a parallel and scalable manner. The Time Series Transformer (TST) (Zerveas et al. 2021) applies the encoder directly to raw time-series tokens with positional encoding to preserve temporal order, while the Time Series Image Transformer (TSiT), adapted from the Vision Transformer (Dosovitskiy et al. 2021), converts time-series segments into patch tokens processed by a Transformer encoder. For both architectures, we tested default, Plus, and multi-head (H8, H12) configurations, yielding nine entries in the benchmark.

Three groups of hybrid architectures were also evaluated. Hybrid CNN+RNN models (LSTM-FCN and GRU-FCN, (Karim et al. 2019)) run an FCN branch in parallel with a recurrent branch and concatenate their representations, combining local convolutional features with sequential modeling. Hybrid Transformer + RNN models feed the output of a Transformer encoder into a recurrent sequence head, integrating global self-attention with explicit temporal ordering; six variants from *tsai* were tested (Transformer + GRU Plus, Bi-GRU Plus, LSTM Plus, Bi-LSTM Plus, RNN Plus, and Bi-RNN Plus). Hybrid Transformer + CNN models use convolutional layers to extract local patterns before Transformer blocks model longer-range dependencies; we evaluated ConvTranPlus (Foumani et al. 2024) in three configurations (Default, Dim Ff 512, and Encoder Learned).

2.6 | Training Protocol and Computational Setup

All 43 models were trained under an identical protocol (Table 1) so that performance differences reflect architectural properties rather than tuning effort. A fixed budget of 500 epochs with no early stopping was adopted, retaining the checkpoint with the lowest validation loss; this avoids the confounding effect of variable stopping points across architectures. For spatial cross-validation, class weights inversely proportional to training-fold class frequencies were applied to address the imbalance introduced by spatial partitioning; uniform weights were used for the balanced random split. No architecture-specific hyperparameter optimisation was performed beyond the default configurations provided by the *tsai* library (Oguiza 2023), except for the Hybrid Transformer+RNN models as detailed below.

TABLE 1 | Training hyperparameters used for all 43 DL models.

Parameter	Value
Optimiser	Adam
Initial learning rate	1×10^{-3}
LR schedule	MultiStepLR at epochs 200, 400 ($\gamma=0.1$)
Total epochs	500 (fixed, no early stopping)
Checkpoint	Lowest validation loss
Batch size	1024
Loss function	Cross-Entropy
Class weights	Balanced (spatial CV)/ Uniform (random split)
Gradient clipping	Max norm = 1.0
Mixed precision	Float16; 6 Transformer-based models in float32
Framework	PyTorch 2.6.0 + tsai 0.4.1
GPU	NVIDIA RTX 4090 (24 GB)

Experiments were conducted on a workstation with an NVIDIA RTX 4090 GPU (24 GB), AMD Ryzen 9, and 64 GB RAM, using PyTorch 2.6.0 (CUDA 12.4). Automatic Mixed Precision (float16) was employed except for six Transformer-based architectures (TST, TST Plus, TSiT Plus, and three Transformer+RNN hybrids) that exhibited numerical overflow and were trained in float32. The six Hybrid Transformer+RNN models required a corrected implementation of the *tsai* library's TransformerRNNPlus encoder, which contained an error in the attention computation, along with adjusted architecture parameters (three encoder layers, feed-forward dimension of 256, eight attention heads, initial learning rate of 1×10^{-4}).

2.7 | Accuracy Analysis

Accuracy analysis evaluated the counts of TP, TN, FP, and FN for each class, generating four complementary metrics:

$$\text{Overall Accuracy} = \frac{\text{TP}+\text{TN}}{\text{TP}+\text{TN}+\text{FP}+\text{FN}} \tag{1}$$

$$\text{Precision} = \frac{\text{TP}}{\text{TP}+\text{FP}} \tag{2}$$

$$\text{Recall} = \frac{\text{TP}}{\text{TP}+\text{FN}} \tag{3}$$

$$\text{F1}-\text{score} = \frac{2\times(\text{Precision}\times\text{Recall})}{\text{Precision}+\text{Recall}} \tag{4}$$

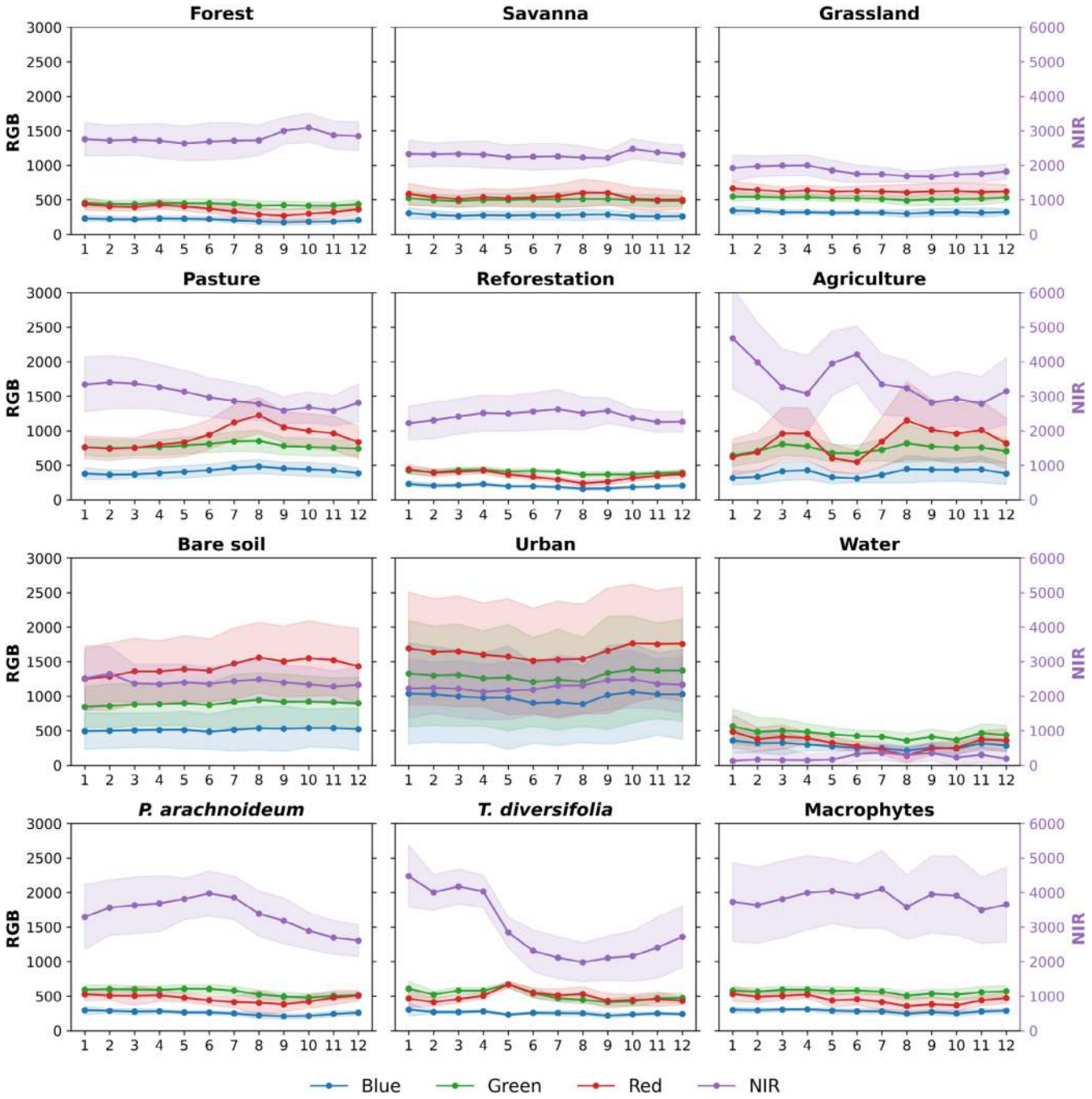


FIGURE 3 | Spectro-temporal profiles (monthly mean ± SD) for 12 land-use/land-cover classes derived from Planet NICFI monthly mosaics (2023). The *x*-axis represents months (1 = January to 12 = December). Mean reflectance for the Blue, Green, and Red bands is shown on the left y-axis (RGB scale), while NIR reflectance is displayed on the right *y*-axis using an independent scale to improve visual comparability. Solid lines represent monthly means and shaded areas indicate ±1SD. Classes: (1) forest formations, (2) savanna formations, (3) grassland formations, (4) pasture, (5) reforestation, (6) agriculture, (7) bare soil, (8) urban area, (9) water, (10) *P. arachnoideum*, (11) *T. diversifolia*, and (12) macrophytes and other wetland vegetations. Shadow is omitted for display brevity.

3 | Results

3.1 | Spectrotemporal Behavior of Targets

Spectrotemporal analysis of the 13 classes (Figure 3) revealed a gradient of phenological distinctiveness. Among natural vegetation, forest formations presented high and stable NIR reflectance throughout the year, savannas showed intermediate NIR with moderate seasonality, and grasslands exhibited the most contrasting behavior: strong NIR oscillation between the rainy and dry seasons, accompanied by greater soil exposure during senescence.

Anthropogenic classes were readily separable: agriculture displayed the most dynamic profile due to planting–harvest cycles, urban areas and bare soil presented low and

stable reflectance, and reforestation resembled forest but with greater variability across plots of different ages. Water had near-zero NIR with minimal temporal variation; shadow (an auxiliary class included to reduce classification errors) showed uniformly low values across all bands; and macrophytes maintained high NIR year-round but with wide standard deviations reflecting water-level fluctuations and spatial heterogeneity in cover density.

Pteridium arachnoideum shows a dense and structurally homogeneous frond canopy that results in elevated Green and NIR reflectance throughout the first half of the year, with a peak around June–July and a progressive decline from August onwards. This behavior is consistent with the frequent occurrence of *P. arachnoideum* in humid environments, such as riparian margins, where soil moisture persists into the early dry season, sustaining photosynthetic activity for longer before a more marked decline in subsequent months. This behavior overlaps with the forest formation class during some rainy months, leading to confusion between the two classes. The standard deviation is also wider than in other vegetation formations, reflecting the heterogeneity resulting from mosaics of variable density, generally in edge areas, gaps, and disturbed environments.

The flowering of the Mexican sunflower (*T. diversifolia*), between April and June, presents a characteristic yellow color that is visually dominant in the field. The flowering behavior is detected in the spectral data, which show a progressive reduction in NIR, indicating a decrease in leaf vigor and green leaf density, concomitant with a slight relative increase in the red and green bands, resulting in the reflectance typical of yellow flowers. This flowering behavior gives the Mexican sunflower a characteristic and easily identifiable phenological signature.

3.2 | Comparative Performance of Deep Learning Models

Table 2 lists the F1-score under random stratified split and the full metric set (OA, P, R, F1) under spatial cross-validation for the 43 DL time-series models (mean ± standard deviation across five seeds or folds). Because the dataset is balanced, OA ≈ P ≈ R ≈ F1 under random splitting; the discussion below focuses on F1 for brevity. The complete experiment ($43 \times 5 = 215$ runs per strategy) required approximately 4 h (random) and 4.5 h (spatial CV) on the RTX 4090, with individual training times ranging from 50 to 120 s.

Under random splitting, pure CNNs achieved the highest group-averaged F1 (98.0%), with XceptionTime leading at 98.8% ± 0.1%; only TCN fell below 97% (95.7% ± 0.7%). Hybrid CNN + RNN models were equally competitive (group average 98.4%), with LSTM-FCN at 98.5% ± 0.1%. Transformers ranked third (group average 96.6%), led by TST Plus H8 (98.6% ± 0.1%), although TSiT Plus variants scored noticeably lower (92.9%–93.3%). Hybrid T + CNN models achieved 97.8%–97.9%. Hybrid T + RNN models, with the corrected implementation (Section 2.6), achieved competitive results (group average 98.2%). RNNs exhibited the widest intra-group variation (89.9%–97.9%, group average 92.9%), with attention-based variants (97.9%) performing on par with the best CNNs while basic recurrent architectures ranged from 89.9% to 91.3%. Overall, the group ranking by mean F1 was Hybrid CNN + RNN (98.4%) ≈ Hybrid T + RNN (98.2%) ≈ CNN (98.0%) > Hybrid T + CNN (97.8%) > Transformer (96.6%) > RNN (92.9%).

Under spatial cross-validation, performance dropped substantially across all groups, revealing architecture-dependent gaps. CNNs maintained the strongest spatially independent performance, with FCN achieving the highest test F1 (81.6% ± 1.3%), followed by ResNet Plus (81.3% ± 3.1%) and FCN Plus (81.1% ± 2.3%), with inflation from random splitting ranging from 17 to 23 pp. Hybrid CNN + RNN models performed competitively (LSTM-FCN: 81.4% ± 2.3%; GRU-FCN: 81.3% ± 2.5%), ranking among the top architectures overall. Among Transformers, TST Default achieved the best spatial result (80.7% ± 2.5%), although TSiT variants dropped substantially (68.0%–68.9%). Hybrid T + CNN models achieved 77.8%–79.1% test F1. Hybrid T + RNN models achieved 75.7%–76.8%, comparable to pure RNNs (70.8%–75.4%), with T + Bi-GRU Plus reaching the best result in the group (76.8% ± 4.5%). RNNs ranged from 70.8% to 75.4%, with attention mechanisms improving spatial generalization by 3–4 pp. Overall, the inflation ranged from 16 to 25 pp. across all six groups, directly quantifying the degree to which spatial autocorrelation inflates performance under random splitting.

The two target species respond differently to spatial independence (Table 3). *Tithonia diversifolia* retains high precision (∼95%–98%) and recall (∼93%–96%), yielding F1 ∼ 93%–95% (gap ∼4 pp); while *P. arachnoideum* drops more substantially (F1 > 71%–79%, gap ∼19–23 pp), with recall remaining high (∼91%) but precision falling to ∼63%–73%. The per-class breakdown (Table 4) shows that spatial stability varies substantially across the 13 classes, from near-perfect transfer for Water (spatial F1 = 97.3%) and Shadow (93.9%) to large drops for Pasture (65.0%, $\Delta = 32.6$ pp) and Macrophytes (70.3%, $\Delta = 28.7$ pp). Forest maintains high recall (83%) but lower precision (72%).

3.3 | Confusion Matrices and Per-Class Accuracy

Figure 4 contrasts the row-normalized confusion matrices for FCN under random splitting and spatial CV. Under random splitting (Figure 4a), all 13 classes exceed 96% diagonal values. Residual errors are concentrated in ecologically similar transitions: approximately 1% of forest samples are assigned to *P. arachnoideum*, and slight confusion occurs between savanna and grassland and between pasture and bare soil. *Tithonia diversifolia* achieves near-perfect classification (> 99%).

Under spatial CV (Figure 4b), inter-class confusion amplifies substantially. Pasture drops from 98% to 72%, bare soil from 97% to 73%, and forest from 97% to 83%. The confusion between forest and *P. arachnoideum* becomes particularly pronounced, with 9% of forest samples assigned to *P. arachnoideum* compared to 1% under random splitting. Classes with distinctive spectral-temporal signatures (water, shadow, *T. diversifolia*) retain values of at least 93% under both evaluation strategies.

TABLE 2 | Performance of 43 DL models under random stratified split (5 seeds) and spatial cross-validation (5 folds), mean ± SD (%). Random split: Only F1 shown (OA ≈ P ≈ R ≈ F1 on balanced data). Spatial CV: Metrics on held-out test fold. Best per group in bold.

	Random	Spatial CV			
Model	**F1**	**OA**	**P**	**R**	**F1**
CNNs (11 models)					
XceptionTime	**98.8 ± 0.1**	82.3 ± 1.7	81.5 ± 1.6	84.9 ± 2.1	81.0 ± 2.0
InceptionTime	98.7 ± 0.1	82.4 ± 2.8	81.2 ± 2.8	85.1 ± 2.7	81.0 ± 3.2
InceptionTime Plus	98.7 ± 0.2	81.1 ± 3.1	79.8 ± 1.6	83.0 ± 1.5	79.3 ± 0.6
ResNet	98.5 ± 0.3	81.9 ± 2.7	80.4 ± 2.4	84.2 ± 1.9	80.2 ± 2.2
ResNet Plus	98.5 ± 0.3	82.9 ± 3.3	81.2 ± 3.2	84.9 ± 2.4	81.3 ± 3.1
FCN	98.4 ± 0.1	**82.9 ± 2.6**	**81.7 ± 1.7**	**85.1 ± 1.7**	**81.6 ± 1.3**
FCN Plus	98.4 ± 0.1	82.9 ± 3.6	80.9 ± 2.5	84.8 ± 1.7	81.1 ± 2.3
OmniScaleCNN	98.3 ± 0.2	81.7 ± 3.0	81.2 ± 2.7	84.0 ± 2.4	80.4 ± 2.4
XCM Plus	97.1 ± 0.2	80.1 ± 4.1	78.4 ± 4.1	82.1 ± 3.8	77.8 ± 4.4
XCM	97.1 ± 0.2	79.2 ± 1.8	77.3 ± 1.8	80.7 ± 2.5	76.9 ± 2.1
TCN	95.7 ± 0.7	74.9 ± 4.3	73.7 ± 2.5	78.2 ± 3.5	73.1 ± 4.2
RNNs (12 models)					
LSTM Attention	97.9 ± 0.4	77.6 ± 2.6	75.2 ± 2.6	79.3 ± 2.2	74.6 ± 2.2
Bi-LSTM Attention	**97.9 ± 0.3**	75.9 ± 4.5	75.2 ± 3.6	78.8 ± 2.7	74.0 ± 3.9
Bi-GRU Attention	97.7 ± 0.5	77.2 ± 3.8	76.2 ± 2.5	79.7 ± 1.6	74.8 ± 2.2
GRU Attention	97.3 ± 0.6	**79.0 ± 2.8**	**76.4 ± 1.5**	**79.8 ± 2.0**	**75.4 ± 1.9**
Bi-LSTM Plus	91.3 ± 0.6	75.7 ± 3.3	73.6 ± 3.6	75.0 ± 4.2	71.7 ± 3.7
Bi-LSTM	91.2 ± 0.7	77.0 ± 3.8	74.2 ± 3.4	76.2 ± 3.4	73.0 ± 3.5
GRU	91.0 ± 0.8	76.3 ± 4.5	72.5 ± 4.8	74.4 ± 4.9	71.0 ± 4.9
Bi-GRU	90.9 ± 0.5	76.0 ± 4.4	74.2 ± 4.3	75.5 ± 3.8	72.4 ± 4.2
LSTM Plus	90.4 ± 1.3	75.5 ± 4.0	72.1 ± 4.6	74.7 ± 2.9	70.8 ± 3.9
Bi-GRU Plus	90.3 ± 0.6	76.6 ± 3.2	74.0 ± 3.8	76.2 ± 3.9	72.7 ± 3.4
GRU Plus	89.9 ± 1.1	75.7 ± 4.6	73.1 ± 3.0	76.1 ± 4.3	72.0 ± 3.7
LSTM	89.9 ± 0.9	76.0 ± 3.0	72.7 ± 2.4	74.8 ± 4.1	71.1 ± 2.9
Transformers (9 models)					
TST Plus	98.6 ± 0.1	80.5 ± 4.0	79.9 ± 4.0	83.4 ± 3.5	79.2 ± 4.1
TST Plus H8	**98.6 ± 0.1**	80.8 ± 3.9	80.1 ± 2.8	83.5 ± 2.4	79.6 ± 3.0
TST Plus H12	98.5 ± 0.1	81.5 ± 3.7	80.4 ± 2.7	84.0 ± 2.4	80.1 ± 2.6
TST H12	98.4 ± 0.3	82.2 ± 3.7	80.5 ± 3.0	83.7 ± 2.7	80.4 ± 3.8
TST Default	98.3 ± 0.2	**82.7 ± 4.5**	**80.9 ± 2.2**	**84.5 ± 2.1**	**80.7 ± 2.5**
TST H8	98.2 ± 0.2	82.4 ± 2.7	80.4 ± 2.7	84.7 ± 2.8	80.4 ± 3.1
TSiT Plus	93.4 ± 0.4	70.8 ± 5.2	69.2 ± 3.0	73.4 ± 2.8	68.0 ± 4.0
TSiT Plus H8	93.0 ± 0.5	71.1 ± 5.7	68.9 ± 3.0	73.6 ± 4.6	68.1 ± 5.1
TSiT Plus H12	92.9 ± 0.4	71.7 ± 4.4	69.6 ± 2.3	73.7 ± 2.1	68.9 ± 3.3
Hybrid T+RNN (6 models)					
T + Bi-RNN Plus	**98.4 ± 0.1**	77.4 ± 4.2	76.7 ± 3.2	81.3 ± 2.6	76.0 ± 4.0
T + Bi-GRU Plus	98.2 ± 0.1	**77.7 ± 5.0**	**77.6 ± 3.2**	**82.0 ± 3.5**	**76.8 ± 4.5**
T + RNN Plus	98.2 ± 0.2	77.6 ± 4.4	76.3 ± 3.6	81.5 ± 3.4	76.0 ± 4.5

(Continues)

TABLE 2 | (Continued)

	Random	Spatial CV			
Model	**F1**	**OA**	**P**	**R**	**F1**
T + GRU Plus	98.1 ± 0.1	77.4 ± 5.0	76.5 ± 3.7	81.5 ± 4.1	76.0 ± 5.1
T + Bi-LSTM Plus	98.1 ± 0.1	77.3 ± 4.4	76.8 ± 3.0	80.9 ± 2.4	75.7 ± 3.8
T + LSTM Plus	98.1 ± 0.2	77.5 ± 5.0	76.8 ± 3.5	81.6 ± 3.6	76.0 ± 4.8
Hybrid T+CNN (3 models)					
ConvTran Plus Ff 512	**97.9 ± 0.2**	80.4 ± 3.6	78.3 ± 2.2	82.5 ± 2.0	78.4 ± 2.4
ConvTran Plus	97.8 ± 0.2	**81.1 ± 3.4**	**79.1 ± 3.1**	**83.5 ± 1.7**	**79.1 ± 2.1**
ConvTran Plus Enc. Learned	97.8 ± 0.2	80.0 ± 2.8	78.2 ± 2.2	82.2 ± 2.3	77.8 ± 2.2
Hybrid CNN+RNN (2 models)					
LSTM-FCN	**98.5 ± 0.1**	**83.0 ± 3.6**	**81.2 ± 2.6**	**85.0 ± 1.8**	**81.4 ± 2.3**
GRU-FCN	98.3 ± 0.2	82.5 ± 3.4	81.6 ± 2.8	84.8 ± 1.7	81.3 ± 2.5

3.4 | Spatial Mapping Results

Figure 5 shows the wall-to-wall classification of land use and land cover produced by majority-vote ensemble of five FCN models (one per random seed), the most spatially robust architecture (Section 3.2), in the Federal District, illustrating the spatial distribution of all 13 classes. Pixel-wise agreement among the five seeds was high: 72.2% of valid pixels received unanimous votes (5/5), and 85.9% had at least 4/5 agreement, indicating strong ensemble consistency. The classification delineates urban areas, reforestation, and water bodies. Agricultural areas are concentrated in the eastern portion, interspersed with pastures and exposed soil. Areas designated for conservation (e.g., Águas Emendadas Ecological Station, Brasília National Park, and the IBGE Ecological Reserve) show their extensions covered by continuous natural vegetation formations.

The studied species exhibit distinct patterns (Figure 6). *Pteridium arachnoideum* is more concentrated in forest fragment edges and areas transitioning to savannas, where disturbance creates conditions favorable to its super-dominant expansion. *Tithonia diversifolia* is primarily associated with highway margins and peri-urban zones, with a high occurrence in areas of anthropogenic disturbance. In conservation areas such as the Brasília National Forest and National Park, areas classified as *P. arachnoideum* concentrate primarily along the edges of riparian environments and forest fragments, which should be prioritized for monitoring, particularly following fire events.

4 | Discussion

4.1 | Methodological Contributions and Model Performance

Remote-sensing studies on encroaching plants increasingly adopt DL; yet, most works still rely on UAV imagery and single-date segmentation or detection. Single-date 2D CNN segmentation typically requires dense, pixel-level polygon masks. In heterogeneous savanna mosaics, precise delineation is difficult and prone to boundary noise, making a point-based sampling strategy coupled with time-series classification a more appropriate and scalable approach. By contrast, time-series DL approaches remain scarce and are concentrated in a few contexts, chiefly aquatic/coastal or alpine wetlands, such as *Spartina* (Tian et al. 2020; Min et al. 2025), leafy spurge (Lake et al. 2022), and *Pedicularis* (Zhu et al. 2025). Building on this gap, our study benchmarks 43 DL models across six families (CNNs, RNNs, Transformers, Hybrid T + RNN, Hybrid T + CNN, and Hybrid CNN + RNN) on monthly satellite time series in a heterogeneous tropical savanna. It adopts a 13-class LULC scheme to expose and mitigate confusion with spectrally similar targets, going beyond the small (often 3–6) model comparisons and conventional ML baselines highlighted by recent reviews (Cheng et al. 2023).

Under random splitting, the results demonstrate that the combined use of Planet NICFI time series with DL classifiers enables accurate detection of target plants in a heterogeneous tropical savanna. CNNs, Transformers, and hybrid architectures achieved the highest accuracy (Table 2), consistent with their capacity to learn multi-scale temporal filters (CNNs), long-range dependencies via self-attention (Transformers), or complementary feature combinations (hybrids), all of which are critical to separating phenological signals in seasonal ecosystems such as the Cerrado. Among the RNN methods, attention mechanisms improved the results: by assigning greater weight to phenologically critical periods, these models better capture discriminative temporal features within the 12-month series. Hybrid CNN + RNN and Transformer + RNN designs were equally competitive, suggesting complementarity between local (convolutional) and sequential (recurrent) temporal features, although gains over the best pure models were marginal in our dataset.

The performance among architectural families is consistent with the structural properties of the 12-month phenological signal. Temporal CNNs have proven to be highly effective when discriminative information is encoded in the morphological form of the signal, rather than in long autoregressive dependencies, since convolutions act as hierarchical shape detectors in fixed-length sequences (Ismail Fawaz et al. 2019). In seasonal ecosystems such as the Cerrado, discrimination primarily relies on the morphology of annual trajectories and

TABLE 3 | Per-species detection under random split and spatial CV (mean ± SD, %). Best spatial-CV model per group. Random P ≈ R ≈ F1 (balanced); only F1 shown. Ordered by spatial F1.

		Random	Spatial CV		
Model	**Group**	**F1**	**P**	**R**	**F1**
P. arachnoideum					
LSTM-FCN	CNN + RNN	98.5	73.0 ± 17.9	**92.4 ± 10.8**	**79.3 ± 8.8**
T + Bi-GRU Plus	T + RNN	98.9	70.8 ± 23.4	92.1 ± 10.6	76.6 ± 15.4
FCN	CNN	98.5	71.0 ± 21.1	90.9 ± 14.5	76.2 ± 12.0
TST Default	Transf.	98.2	67.3 ± 22.2	90.8 ± 11.3	73.6 ± 11.1
ConvTran Plus	T + CNN	98.0	66.9 ± 23.0	88.3 ± 15.4	71.5 ± 15.7
GRU Attention	RNN	97.5	63.6 ± 25.8	91.8 ± 9.3	70.8 ± 17.0
T. diversifolia					
FCN	CNN	99.7	**98.5 ± 1.6**	93.1 ± 8.9	**95.5 ± 4.6**
T + Bi-RNN Plus	T + RNN	99.7	95.0 ± 7.7	**96.3 ± 7.2**	95.3 ± 4.9
TST Default	Transf.	99.7	95.9 ± 3.0	94.6 ± 7.4	95.0 ± 3.0
ConvTran Plus	T + CNN	99.5	98.2 ± 1.1	90.7 ± 13.7	93.7 ± 8.3
GRU Attention	RNN	99.6	93.5 ± 5.2	94.3 ± 7.9	93.6 ± 4.4
LSTM-FCN	CNN + RNN	99.8	95.5 ± 5.5	92.7 ± 11.0	93.6 ± 6.5

Note: The bold values indicate the best performance for each metric among the evaluated models.

TABLE 4 | Per-class FCN metrics under random split and spatial CV (mean ± std., %). Random P ≈ R ≈ F1 (balanced); only F1 shown.

	Random	Spatial CV		
Class	**F1**	**P**	**R**	**F1**
Target species				
T. diversifolia	99.7 ± 0.2	98.5 ± 1.6	93.1 ± 8.9	95.5 ± 4.6
P. arachnoideum	98.5 ± 0.4	71.0 ± 21.1	90.9 ± 14.5	76.2 ± 12.0
Natural vegetation				
Grassland	98.6 ± 0.5	89.6 ± 13.2	83.2 ± 10.3	86.1 ± 11.2
Savanna	97.1 ± 1.0	80.2 ± 14.5	81.4 ± 15.1	79.5 ± 11.4
Forest	97.2 ± 0.8	71.8 ± 16.1	83.1 ± 21.0	73.7 ± 13.3
Anthropogenic/managed				
Urban	98.3 ± 0.6	88.6 ± 8.4	94.1 ± 8.4	90.6 ± 3.9
Reforestation	98.7 ± 0.3	88.3 ± 13.4	78.5 ± 14.1	82.3 ± 11.8
Agriculture	98.7 ± 0.4	71.5 ± 10.5	84.7 ± 14.8	76.8 ± 10.6
Bare soil	96.9 ± 0.6	76.3 ± 8.8	73.1 ± 23.7	72.9 ± 16.3
Pasture	97.6 ± 0.6	64.1 ± 21.1	72.2 ± 6.4	65.0 ± 10.4
Other				
Water	99.8 ± 0.2	96.1 ± 5.1	98.5 ± 1.5	97.3 ± 3.1
Shadow	99.3 ± 0.3	91.4 ± 6.1	96.8 ± 4.7	93.9 ± 4.5
Macrophytes	99.0 ± 0.5	75.0 ± 16.0	76.3 ± 29.1	70.3 ± 21.6

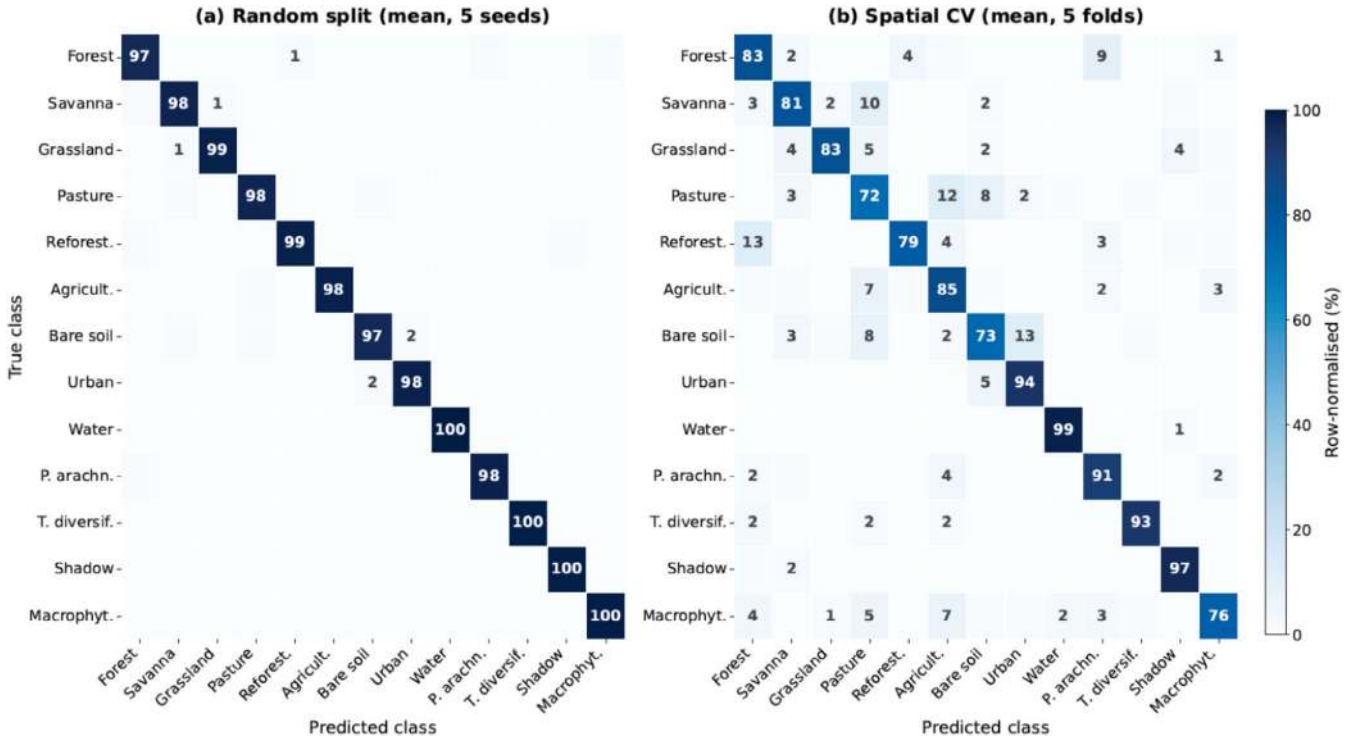


FIGURE 4 | Row-normalized confusion matrices (%) for FCN, averaged over (a) five random seeds and (b) five spatial CV folds. The *y*-axis shows true classes and the *x*-axis predicted classes; colors range from 0 (white) to 100 (blue). Class indices: (1) forest, (2) savanna, (3) grassland, (4) pasture, (5) reforestation, (6) agriculture, (7) bare soil, (8) urban, (9) water, (10) *P. arachnoideum*, (11) *T. diversifolia*, (12) shadow, and (13) macrophytes and other wetland vegetations.

associated phenological features, rather than on extended temporal dependencies. Transformers extend this capacity through self-attention mechanisms (Vaswani et al. 2017), supporting direct comparisons across non-adjacent months and modeling global temporal relationships. The advantage of this architecture is that the classes differ in the timing or persistence of spectral signals throughout the annual cycle. In contrast, RNNs rely on recursive state updates that compress temporal information into evolving hidden representations, which may be less suited to short, globally structured seasonal sequences such as our data. Zhong et al. (2019) reported superior performance of temporal convolutional models compared with LSTM in crop classification, attributing this to the ability of convolutions to capture multi-scale seasonal patterns without relying on recursive state updates. Additionally, the review by Cheng et al. (2023) documents the increasing adoption of convolutional and attention-based architectures in multitemporal remote sensing classification, underscoring their suitability for structured temporal signals. In this context, the inductive biases of CNNs and Transformers appear better aligned with annual phenological trajectories than those of RNNs.

The observed performance can be interpreted in light of the biophysical consistency between phenological dynamics and spectral response. The four spectral bands available in the Planet NICFI product (Blue, Green, Red, and NIR) are sufficient to capture the key biophysical signals that differentiate the target species both from each other and from other LULC classes. As described in Section 3.1, the target species exhibit distinct phenological behaviors: *T. diversifolia* is characterized by a marked flowering phase between April and June associated with increased Green and Red reflectance and reduced NIR, whereas *P. arachnoideum* forms a dense frond canopy with elevated Green and NIR reflectance during the first half of the year, followed by a seasonal decline. These phenological patterns generate a temporally coherent green-up and flowering signal within the 12-month series. Thus, DL models do not rely solely on instantaneous spectral separability but instead learn characteristic temporal trajectories associated with flowering, green-up, and senescence. The high performance in spatial cross-validation (F1≈76%–95%) demonstrates that the monthly phenological dynamics of the four Planet NICFI bands are sufficient to achieve accurate discrimination in a multiclass framework. These findings reinforce the importance of time-series architectures in phenology-driven ecosystems, particularly where visual similarity between targets and native formations is high. In addition to model selection, we adopted a 13-class land-use/land-cover scheme rather than a simplified binary "target vs. non-target" configuration. The larger number of classes reduces systematic confusion with spectrally and phenologically similar targets (e.g., crops, pastures, forest edges), makes error sources explicit, and guides a more targeted selection of training samples and post hoc corrections.

4.2 | Spatial Autocorrelation Effects

The comparison between random and spatially independent evaluation is perhaps the most consequential result of this study. As shown in Section 3.2, the inflation ranged from 16 to 25 pp. across all six architecture groups. This inflation arises because nearby samples share spectral-temporal characteristics due to

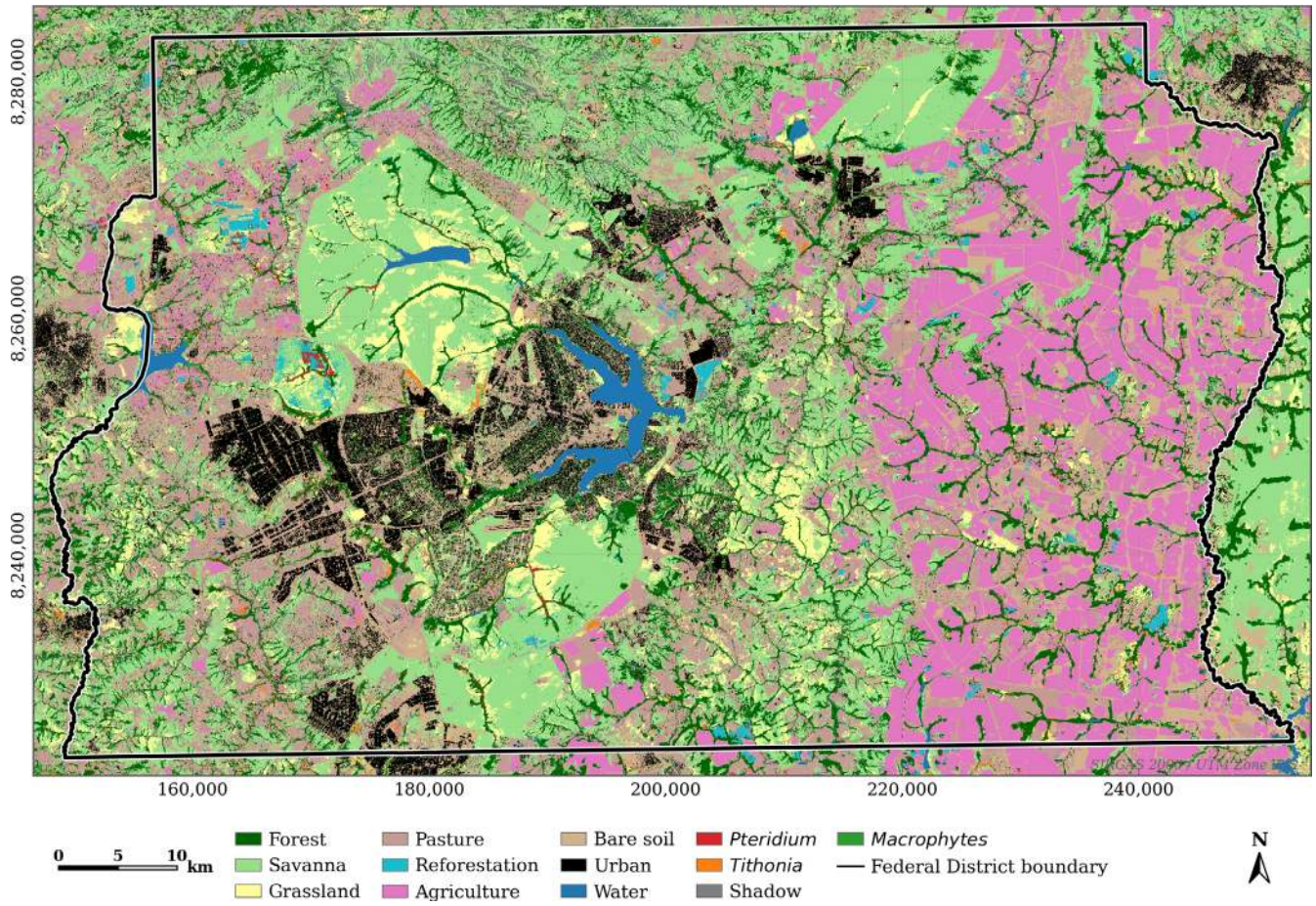


FIGURE 5 | Land use and land cover map of the study area, generated by majority-vote ensemble of five FCN models trained on Planet NICFI monthly composites (2023). The map shows the main land-use and land-cover classes, as well as the occurrence of the target species *P. arachnoideum* and *T. diversifolia*.

common environmental conditions (soil type, microclimate, disturbance history). When training and test sets draw from the same spatial neighborhood, models can exploit these location-specific patterns without learning generalisable phenological signatures. Spatial CV, by holding out entire geographic regions, strips away this source of optimistic bias.

The per-class breakdown (Table 4) shows that this bias is not uniform. Classes with highly distinctive signatures (Water, Shadow, *T. diversifolia*) transfer reliably across regions, while classes whose spectral characteristics depend on local management or hydrological conditions (Pasture, Macrophytes) suffer the steepest drops. Natural vegetation classes (Forest, Savanna) occupy an intermediate position, reflecting regional variation in species composition and canopy structure.

The two target species exhibit contrasting spatial behavior (Section 3.2, Table 3). The precision–recall decomposition for *P. arachnoideum* (high recall but substantially lower precision) indicates that the model detects most occurrences but generates FPs from spectrally similar forest pixels. This confusion is spatially variable because the NIR overlap identified in Section 3.1 depends on local canopy structure and degradation history; 8.7% of Forest test samples are misclassified as *P. arachnoideum* under spatial CV, compared to just 1% under random splitting. For *T. diversifolia*, the consistently high precision and recall confirm that the diagnostic flowering phenology identified in Section 3.1 transfers across geographic contexts.

The Hybrid Transformer+RNN models, after the implementation correction described in Section 2.6, achieved 75.7%–76.8% spatial F1, comparable to pure RNNs and Transformers, with a random-to-spatial gap of ~22 pp. consistent with the other groups. FCN, a lightweight three-layer convolutional architecture, outperforms deeper models under spatial CV despite ranking below them under random splitting (Table 2), a ranking reversal consistent with a bias–variance tradeoff in which greater model capacity enables memorisation of region-specific patterns at the cost of spatial transferability.

For operational deployment, these results argue for selecting simple, well-regularized architectures (FCN, LSTM-FCN) when spatial transferability is the priority. We also recommend that future benchmarking studies routinely include spatial CV alongside random splits to obtain realistic performance estimates.

4.3 | Management and Monitoring Implications

From a management perspective, the spatial patterns indicate different surveillance strategies. *Tithonia diversifolia* concentrates along roads, agricultural edges and peri-urban



FIGURE 6 | Detection examples of the two target species in the Federal District. Left half: Invasive alien Mexican sunflower, *T. diversifolia*, in peri-urban areas (Planet NICFI RGB composite from May 2023, peak flowering). (a, b) RGB composites at two sites; (e, f) same areas with majority-vote FCN classification overlay (orange), aligned with the yellow–green patches typical of the species' flowering canopy. Right half: Native super-dominant bracken fern, *P. arachnoideum*, in protected areas (Planet NICFI RGB composite from July 2023, dry season). (c) Brasília National Forest; (d) Brasília National Park; (g, h) corresponding FCN overlay (red), with occurrences concentrated along riparian margins and forest–savanna transition zones. Each panel covers approximately 3.6 × 3.6 km.

zones; these linear, accessible *features* are amenable to routine, low-cost patrols informed by monthly alerts. *Pteridium arachnoideum* clusters along forest–savanna transitions and riparian margins, particularly in burned or repeatedly disturbed sites; here, edge-targeted monitoring and post-fire assessments can prioritize control. The history of severe fires in conservation areas (e.g., Brasília National Forest in 2016, 2017, 2024; Brasília National Park in 2010: ~15,600 ha, 2022: 7700 ha, 2024: 14,000 ha) creates conditions favorable for *P. arachnoideum* expansion. This species acts as an ecological filter, hindering the regeneration of tree species through its dense frond canopy and extensive rhizome system. Post-fire monitoring in these areas is therefore strategic for containing the expansion of the species. Because our multiclass design reduces confusion with spectrally similar classes (e.g., crops, pastures), outputs can be used to triage field teams with fewer FPs than a binary pipeline. Taken together, the workflow provides a repeatable early-warning system for agencies to plan interventions while minimizing survey effort.

The spatial CV results refine these recommendations. Because *T. diversifolia* detection transfers well across regions (F1 ~ 95%, Table 3), a single trained model can be deployed for monitoring across the studied region with high confidence. For *P. arachnoideum*, the precision–recall imbalance reported (recall ~91% but precision ~65%–70%, Table 3) has practical implications: high recall means few infestations go undetected, but lower precision implies that field teams will encounter some false alarms, a trade-off generally acceptable in conservation, where missing an actual infestation is costlier than investigating a false alert. Agencies deploying models for *P. arachnoideum* in new regions should plan for local calibration with a modest set of ground-truth samples to restore precision.

4.4 | Limitations and Future Directions

This study presents limitations related to both the data used and the methodological choices adopted. Regarding the data, there are four main factors. First, the spatial resolution (4.77 m) may not identify small, sparse, or subcanopy occurrences, especially for *P. arachnoideum* under partial canopy cover. Second, transition areas can be challenging due to spectral mixing, with varying target contributions. Third, the analysis is limited to the Federal District; although performance was high under random splitting, the spatial CV results demonstrate that domain shift substantially reduces performance, suggesting that transferability to completely new regions may require region-specific calibration or fine-tuning. Fourth, although the NICFI monthly composites minimize cloud contamination through best-pixel selection, residual atmospheric effects may persist in regions with persistent cloud cover, particularly during the Cerrado wet season, potentially introducing noise in the spectral-temporal signatures. From a methodological standpoint, DL models require GPU-based computing infrastructure, which may limit their adoption among groups with limited computing resources. Furthermore, most architectures were trained with the default hyperparameters provided by the *tsai* library without architecture-specific tuning (except for the six Hybrid T + RNN models, which required implementation corrections

and configuration adjustments as described in Section 2.6); while this ensures a largely fair comparison reflecting architectural differences rather than tuning effort, it may underestimate the potential of models with more configurable parameters (e.g., Transformers with variable numbers of heads and layers), and future work could investigate whether architecture-specific optimisation alters the relative rankings.

As a natural extension of this research, future studies may expand the analysis to an interannual framework. The present study restricted the analysis to a single year to isolate the relative behavior of the architectures, the central focus of this research, and to reduce confounding factors, such as interannual variability. However, restricting the analysis to a single year does not allow us to assess how performance responds to interannual climatic variability. Differences in rainfall and temperature may shift phenological timing, affect spectral intensity, or modify vegetation structure after disturbances such as fire or severe drought. These factors may affect not only absolute performance values but also the stability of the learned spectro-temporal representations over time. It is expected that the relative ranking of the architectures will be less sensitive to these variations than the absolute metric values, but this hypothesis still needs to be tested. Therefore, incorporating multi-year time series allows us to assess the temporal transferability and model behavior under different climatic and disturbance regimes. It should also be emphasized that, even when limited to a single year, the analysis produces wall-to-wall maps of the spatial distribution of encroaching species under a spatial cross-validation framework. This information is relevant in itself for understanding the extent and spatial pattern of target species occupancy during the analyzed period, independent of interannual transferability.

Along the same lines, broadening the approach to encompass different data sources constitutes a complementary development. Evaluating free images, such as those from Sentinel-2 (10 m, with additional bands) and Sentinel-1 SAR, can increase scalability and reduce dependence on commercial products, especially considering that Planet NICFI images are no longer open access. Furthermore, future work should also investigate spatial transfer learning strategies to improve model generalization across regions and explore ensemble approaches that combine the complementary strengths of different architecture families.

5 | Conclusion

This study demonstrated the effectiveness of Planet NICFI time series combined with DL architectures for detecting encroaching species (*P. arachnoideum* and *T. diversifolia*) in the Cerrado, a topic underexplored in the literature. Forty-three architectures were evaluated in six groups (CNNs, RNNs, Transformers, Hybrid Transformer + RNN, Hybrid Transformer + CNN, and Hybrid CNN + RNN), considering 13 classes in a multiclass approach. Under random stratified splitting, CNNs, Transformers, and hybrid architectures all presented strong results, with F1 scores close to or above 98%. XceptionTime (98.8%) and InceptionTime (98.7%) stood out among CNNs, while TST Plus led the Transformers (98.6%). Hybrid CNN + RNN (LSTM-FCN: 98.5%) and Hybrid Transformer+RNN models (T + Bi-RNN Plus: 98.4%) demonstrated highly competitive performance. However, the introduction of spatial cross-validation revealed that random splitting inflated performance by 16–25 percentage points across all architecture groups. Under spatially independent evaluation, FCN achieved the highest test F1 (81.6%), followed by LSTM-FCN (81.4%) and ResNet Plus (81.3%). These performance gaps, which would have remained hidden without spatially independent evaluation, underscore the critical importance of spatial CV in remote sensing benchmarks. *Tithonia diversifolia* was reliably detected owing to its characteristic flowering and maintained high detectability across spatial regions (test F1 ∼ 95%), while *Pteridium arachnoideum* showed a spectrotemporal pattern closer to forest formations, with more spatially dependent detection (test F1 ∼ 76%). The predicted spatial distribution was consistent with field mapping, validating the approach for operational deployment. These results confirm the critical importance of spatially independent validation in remote sensing studies and provide practical guidance for selecting robust architectures for operational monitoring.

Acknowledgments

The authors are grateful for financial support of the grant from the National Council for Scientific and Technological Development (CNPq) for Professor Osmar Abílio de Carvalho Júnior. This study was partly financed by the Coordination for the Improvement of Higher Education Personnel (CAPES) (Finance Code 001), Research Support Foundation of the Federal District (FAPDF) (Project 00193.00002237/2022-92), CAPES (Finance Code 001), and CNPq (research projects 312608/2021-7, 421413/2023-9, and 421291/2022-2). Finally, we thank the LSIE group and the anonymous reviewers for their valuable contributions to the article.

Funding

This work was supported by Conselho Nacional de Desenvolvimento Científico e Tecnológico (312608/2021-7, 421413/2023-9, 421291/2022-2). Coordenação de Aperfeiçoamento de Pessoal de Nível Superior, 001, Fundação de Apoio à Pesquisa do Distrito Federal, 00193.00002237/2022-92.

Conflicts of Interest

The authors declare no conflicts of interest.

Data Availability Statement

The dataset, code, and pre-computed results of this study are publicly available on GitHub at https://github.com/osmarluiz/encroaching-species-cerrado. The repository includes the labeled dataset (16,250 samples, 13 classes), training notebooks, spatial cross-validation scripts, and output results for all 43 deep learning architectures. The Planet NICFI satellite images used in this study are available in the NICFI program (https://www.nicfi.no/).

References

Ahmed, N., C. Atzberger, and W. Zewdie. 2020. "Integration of Remote Sensing and Bioclimatic Data for Prediction of Invasive Species Distribution in Data-Poor Regions: A Review on Challenges and Opportunities." *Environmental Systems Research* 9, no. 1. https://doi.org/10.1186/s40068-020-00195-0.

Ajao, A. A., and A. N. Moteetee. 2017. "*Tithonia diversifolia* (Hemsl) A. Gray. (Asteraceae: Heliantheae), an Invasive Plant of

Significant Ethnopharmacological Importance: A Review." *South African Journal of Botany* 113: 396–403. https://doi.org/10.1016/j.sajb.2017.09.017.

Asner, G. P., R. F. Hughes, P. M. Vitousek, et al. 2008. "Invasive Plants Transform the Three-Dimensional Structure of Rain Forests." *Proceedings of the National Academy of Sciences of the United States of America* 105, no. 11: 4519–4523. https://doi.org/10.1073/pnas.0710811105.

Bahdanau, D., K. H. Cho, and Y. Bengio. 2015. "Neural Machine Translation by Jointly Learning to Align and Translate." 3rd International Conference on Learning Representations, ICLR 2015 - Conference Track Proceedings, 1–15.

Bai, S., J. Z. Kolter, and V. Koltun. 2018. "An Empirical Evaluation of Generic Convolutional and Recurrent Networks for Sequence Modeling." https://arxiv.org/abs/1803.01271.

Beaury, E. M., E. J. Fusco, M. R. Jackson, et al. 2020. "Incorporating Climate Change Into Invasive Species Management: Insights From Managers." *Biological Invasions* 22, no. 2: 233–252. https://doi.org/10.1007/s10530-019-02087-6.

Berry, Z. C., K. Wevill, and T. J. Curran. 2011. "The Invasive Weed *Lantana camara* Increases Fire Risk in Dry Rainforest by Altering Fuel Beds." *Weed Research* 51, no. 5: 525–533. https://doi.org/10.1111/j.1365-3180.2011.00869.x.

Bradley, B. A. 2014. "Remote Detection of Invasive Plants: A Review of Spectral, Textural and Phenological Approaches." *Biological Invasions* 16, no. 7: 1411–1425. https://doi.org/10.1007/s10530-013-0578-9.

Chen, M., Y. Ke, J. Bai, et al. 2020. "Monitoring Early Stage Invasion of Exotic *Spartina alterniflora* Using Deep-Learning Super-Resolution Techniques Based on Multisource High-Resolution Satellite Imagery: A Case Study in the Yellow River Delta, China." *International Journal of Applied Earth Observation and Geoinformation* 92: 102180. https://doi.org/10.1016/j.jag.2020.102180.

Cheng, X., Y. Sun, W. Zhang, Y. Wang, X. Cao, and Y. Wang. 2023. "Application of Deep Learning in Multitemporal Remote Sensing Image Classification." *Remote Sensing* 15, no. 15: 3859. https://doi.org/10.3390/rs15153859.

Cho, K., B. Van Merriënboer, C. Gulcehre, et al. 2014. "Learning Phrase Representations Using RNN Encoder-Decoder for Statistical Machine Translation." EMNLP 2014–2014 Conference on Empirical Methods in Natural Language Processing, Proceedings of the Conference, 1724–1734. https://doi.org/10.3115/v1/d14-1179.

Cook, D. C., M. B. Thomas, S. A. Cunningham, D. L. Anderson, and P. J. De Barro. 2007. "Predicting the Economic Impact of an Invasive Species on an Ecosystem Service." *Ecological Applications* 17, no. 6: 1832–1840. https://doi.org/10.1890/06-1632.1.

Dosovitskiy, A., L. Beyer, A. Kolesnikov, et al. 2021. "An Image Is Worth 16×16 Words: Transformers for Image Recognition at Scale." ICLR 2021—9th International Conference on Learning Representations, 1–22. https://arxiv.org/abs/2010.11929.

Estabrooks, A., T. Jo, and N. Japkowicz. 2004. "A Multiple Resampling Method for Learning From Imbalanced Data Sets." *Computational Intelligence* 20, no. 1: 18–36. https://doi.org/10.1111/j.0824-7935.2004.t01-1-00228.x.

Evangelista, P. H., T. J. Stohlgren, J. T. Morisette, and S. Kumar. 2009. "Mapping Invasive Tamarisk (*Tamarix*): A Comparison of Single-Scene and Time-Series Analyses of Remotely Sensed Data." *Remote Sensing* 1, no. 3: 519–533. https://doi.org/10.3390/rs1030519.

Fauvel, K., T. Lin, V. Masson, É. Fromont, and A. Termier. 2021. "XCM: An Explainable Convolutional Neural Network for Multivariate Time Series Classification." *Mathematics* 9, no. 23: 3137. https://doi.org/10.3390/math9233137.

Foody, G. M. 2002. "Status of Land Cover Classification Accuracy Assessment." *Remote Sensing of Environment* 80, no. 1: 185–201. https://doi.org/10.1016/S0034-4257(01)00295-4.

Foumani, N. M., C. W. Tan, G. I. Webb, and M. Salehi. 2024. "Improving Position Encoding of Transformers for Multivariate Time Series Classification." *Data Mining and Knowledge Discovery* 38, no. 1: 22–48. https://doi.org/10.1007/s10618-023-00948-2.

Graves, A., and J. Schmidhuber. 2005. "Framewise Phoneme Classification With Bidirectional LSTM and Other Neural Network Architectures." *Neural Networks* 18, no. 5–6: 602–610. https://doi.org/10.1016/j.neunet.2005.06.042.

Große-Stoltenberg, A., C. Werner, C. Hellmann, J. Oldeland, and J. Thiele. 2025. "Quantifying the Spatial Impact of an Invasive *Acacia* on Ecosystem Functioning Using Remote Sensing." *Ecological Indicators* 170: 112928. https://doi.org/10.1016/j.ecolind.2024.112928.

Guerin, N., and G. Durigan. 2015. "Invasion Impact by *Pteridium arachnoideum* (Kaulf.) Maxon (Dennstaedtiaceae) on a Neotropical Savanna." *Acta Botânica Brasílica* 29, no. 2: 213–222. https://doi.org/10.1590/0102-33062014abb3722.

Hao, Z., L. Lin, C. J. Post, and E. A. Mikhailova. 2024. "Monitoring the Spatial–Temporal Distribution of Invasive Plant in Urban Water Using Deep Learning and Remote Sensing Technology." *Ecological Indicators* 162: 112061. https://doi.org/10.1016/j.ecolind.2024.112061.

He, K., X. Zhang, S. Ren, and J. Sun. 2016. "Deep Residual Learning for Image Recognition." 2016 IEEE Conference on Computer Vision and Pattern Recognition (CVPR), 770–778. https://doi.org/10.1109/CVPR.2016.90.

He, K. S., D. Rocchini, M. Neteler, and H. Nagendra. 2011. "Benefits of Hyperspectral Remote Sensing for Tracking Plant Invasions." *Diversity and Distributions* 17, no. 3: 381–392. https://doi.org/10.1111/j.1472-4642.2011.00761.x.

Hochreiter, S., and J. Schmidhuber. 1997. "Long Short-Term Memory." *Neural Computation* 9, no. 8: 1735–1780. https://doi.org/10.1162/neco.1997.9.8.1735.

Huang, C., and G. P. Asner. 2009. "Applications of Remote Sensing to Alien Invasive Plant Studies." *Sensors* 9, no. 6: 4869–4889. https://doi.org/10.3390/s90604869.

Instituto Brasília Ambiental – IBRAM. 2021. *Espécies exóticas invasoras do Distrito Federal*. IBRAM. https://www.ibram.df.gov.br/especies-exoticas-invasoras-do-df/.

IPBES. 2023. *Thematic Assessment Report on Invasive Alien Species and Their Control of the Intergovernmental Science-Policy Platform on Biodiversity and Ecosystem Services*, edited by H. E. Roy, A. Pauchard, P. Stoett, and T. Renard Truong. IPBES Secretariat. https://doi.org/10.5281/zenodo.7430682.

Ismail Fawaz, H., G. Forestier, J. Weber, L. Idoumghar, and P.-A. Muller. 2019. "Deep Learning for Time Series Classification: A Review." *Data Mining and Knowledge Discovery* 33, no. 4: 917–963. https://doi.org/10.1007/s10618-019-00619-1.

Ismail Fawaz, H., B. Lucas, G. Forestier, et al. 2020. "InceptionTime: Finding AlexNet for Time Series Classification." *Data Mining and Knowledge Discovery* 34, no. 6: 1936–1962. https://doi.org/10.1007/s10618-020-00710-y.

Ismail, R., O. Mutanga, and K. Peerbhay. 2016. "The Identification and Remote Detection of Alien Invasive Plants in Commercial Forests: An Overview." *South African Journal of Geomatics* 5, no. 1: 49. https://doi.org/10.4314/sajg.v5i1.4.

Kalisz, S., S. N. Kivlin, and L. Bialic-Murphy. 2021. "Allelopathy Is Pervasive in Invasive Plants." *Biological Invasions* 23: 367–371. https://doi.org/10.1007/s10530-020-02383-6.

Karim, F., S. Majumdar, H. Darabi, and S. Harford. 2019. "Multivariate LSTM-FCNs for Time Series Classification." *Neural Networks* 116: 237–245. https://doi.org/10.1016/j.neunet.2019.04.014.

Kohavi, R. 1995. "A Study of Cross-Validation and Bootstrap for Accuracy Estimation and Model Selection." Proceedings of the 14th International Joint Conference on Artificial Intelligence (IJCAI), pp. 1137–1143.

Lake, T. A., R. D. Briscoe Runquist, and D. A. Moeller. 2022. "Deep Learning Detects Invasive Plant Species Across Complex Landscapes Using Worldview-2 and Planetscope Satellite Imagery." *Remote Sensing in Ecology and Conservation* 8, no. 6: 875–889. https://doi.org/10.1002/rse2.288.

Larson, K. B., and A. R. Tuor. 2021. "Deep Learning Classification of Cheatgrass Invasion in the Western United States Using Biophysical and Remote Sensing Data." *Remote Sensing* 13, no. 7: 1246. https://doi.org/10.3390/rs13071246.

Lazzaro, L., R. Bolpagni, G. Buffa, et al. 2020. "Impact of Invasive Alien Plants on Native Plant Communities and Natura 2000 Habitats: State of the Art, Gap Analysis and Perspectives in Italy." *Journal of Environmental Management* 274: 111140. https://doi.org/10.1016/j.jenvman.2020.111140.

Lea, C., M. D. Flynn, R. Vidal, A. Reiter, and G. D. Hager. 2017. "Temporal Convolutional Networks for Action Segmentation and Detection." 2017 IEEE Conference on Computer Vision and Pattern Recognition (CVPR), 1003–1012. https://doi.org/10.1109/CVPR.2017.113.

Liu, J., M. Dong, S. L. Miao, Z. Y. Li, M. H. Song, and R. Q. Wang. 2006. "Invasive Alien Plants in China: Role of Clonality and Geographical Origin." *Biological Invasions* 8, no. 7: 1461–1470. https://doi.org/10.1007/s10530-005-5838-x.

Luo, X., W. Zhou, W. Wang, Y. Zhu, and J. Deng. 2018. "Attention-Based Relation Extraction With Bidirectional Gated Recurrent Unit and Highway Network in the Analysis of Geological Data." *IEEE Access* 6: 5705–5715. https://doi.org/10.1109/ACCESS.2017.2785229.

Luong, M. T., H. Pham, and C. D. Manning. 2015. "Effective Approaches to Attention-Based Neural Machine Translation." Conference Proceedings—EMNLP 2015: Conference on Empirical Methods in Natural Language Processing, 1412–1421. https://doi.org/10.18653/v1/d15-1166.

Mandle, L., J. L. Bufford, I. B. Schmidt, and C. C. Daehler. 2011. "Woody Exotic Plant Invasions and Fire: Reciprocal Impacts and Consequences for Native Ecosystems." *Biological Invasions* 13, no. 8: 1815–1827. https://doi.org/10.1007/s10530-011-0001-3.

Maney, C., D. Guaras, J. Harrison, et al. 2024. "National Commitments to Aichi Targets and Their Implications for Monitoring the Kunming-Montreal Global Biodiversity Framework." *npj Biodiversity* 3, no. 1: 1–8. https://doi.org/10.1038/s44185-024-00039-5.

Marrs, R. H., and A. S. Watt. 2006. "Biological Flora of the British Isles: *Pteridium aquilinum* (L.) Kuhn." *Journal of Ecology* 94, no. 6: 1272–1321. https://doi.org/10.1111/j.1365-2745.2006.01177.x.

Min, Y., Y. Ke, Z. Zhuo, et al. 2025. "Monitoring *Spartina alterniflora* Removal Dynamics Across Coastal China Using Time Series Sentinel-1 Imagery." *Remote Sensing of Environment* 326: 114813. https://doi.org/10.1016/j.rse.2025.114813.

Mouta, N., R. Silva, S. Pais, et al. 2021. "The Best of Two Worlds—Combining Classifier Fusion and Ecological Models to Map and Explain Landscape Invasion by an Alien Shrub." *Remote Sensing* 13, no. 16: 3287. https://doi.org/10.3390/rs13163287.

Muoghalu, J. I., and D. K. Chuba. 2005. "Seed Germination and Reproductive Strategies of *Tithonia diversifolia* (Hemsl.) Gray and *Tithonia rotundifolia* (P.M) Blake." *Applied Ecology and Environmental Research* 3, no. 1: 39–46. https://doi.org/10.15666/aeer/0301_039046.

Myers, N., R. A. Mittermeier, C. G. Mittermeier, G. A. B. da Fonseca, and J. Kent. 2000. "Biodiversity Hotspots for Conservation Priorities." *Nature* 403, no. 6772: 853–858. https://doi.org/10.1038/35002501.

NICFI. 2024. "Norway's International Climate and Forest Initiative (NICFI)." https://www.nicfi.no/.

Niphadkar, M., and H. Nagendra. 2016. "Remote Sensing of Invasive Plants: Incorporating Functional Traits Into the Picture." *International Journal of Remote Sensing* 37, no. 13: 3074–3085. https://doi.org/10.1080/01431161.2016.1193795.

Nunes, L. J. R., M. A. M. Raposo, C. I. R. Meireles, C. J. Pinto Gomes, and N. M. C. Almeida Ribeiro. 2020. "Fire as a Selection Agent for the Dissemination of Invasive Species: Case Study on the Evolution of Forest Coverage." *Environments* 7, no. 8: 1–14. https://doi.org/10.3390/environments7080057.

Oguiza, I. 2023. "TSAI—A State-of-the-Art Deep Learning Library for Time Series and Sequential Data." GitHub. https://github.com/timeseriesAI/tsai.

Pivello, V. R., M. V. Vieira, M. T. Grombone-Guaratini, and D. M. S. Matos. 2018. "Thinking About Super-Dominant Populations of Native Species—Examples From Brazil." *Perspectives in Ecology and Conservation* 16, no. 2: 74–82. https://doi.org/10.1016/j.pecon.2018.04.001.

Planet Team. 2024. "Planet Application Program Interface: In Space for Life on Earth." https://api.planet.com.

Ploton, P., F. Mortier, M. Réjou-Méchain, et al. 2020. "Spatial Validation Reveals Poor Predictive Performance of Large-Scale Ecological Mapping Models." *Nature Communications* 11: 4540. https://doi.org/10.1038/s41467-020-18321-y.

Pyšek, P., P. E. Hulme, D. Simberloff, et al. 2020. "Scientists' Warning on Invasive Alien Species." *Biological Reviews* 95, no. 6: 1511–1534. https://doi.org/10.1111/brv.12627.

Rahimian, E., S. Zabihi, S. F. Atashzar, A. Asif, and A. Mohammadi. 2020. "XceptionTime: Independent Time-Window Xceptiontime Architecture for Hand Gesture Classification." In: ICASSP 2020–2020 IEEE International Conference on Acoustics, Speech and Signal Processing, 1304–1308. https://doi.org/10.1109/ICASSP40776.2020.9054586.

Rakgoale, P. B., and S. N. Ngetar. 2024. "Detecting Invasive Alien Plant Species Using Remote Sensing, Machine Learning and Deep Learning: A Systematic Review." *Journal of Sensors* 2024, no. 1. https://doi.org/10.1155/2024/8854675.

Ribeiro, J. F., and B. M. T. Walter. 1998. "Fitofisionomias do bioma Cerrado." In *Cerrado: Ambiente e flora*, edited by S. M. Sano and S. P. de Almeida, 89–166. Embrapa-CPAC.

Roberts, D. R., V. Bahn, S. Ciuti, et al. 2017. "Cross-Validation Strategies for Data With Temporal, Spatial, Hierarchical, or Phylogenetic Structure." *Ecography* 40, no. 8: 913–929. https://doi.org/10.1111/ecog.02881.

Rocchini, D., V. Andreo, M. Förster, et al. 2015. "Potential of Remote Sensing to Predict Species Invasions." *Progress in Physical Geography: Earth and Environment* 39, no. 3: 283–309. https://doi.org/10.1177/0309133315574659.

Royimani, L., O. Mutanga, J. Odindi, T. Dube, and T. N. Matongera. 2019. "Advancements in Satellite Remote Sensing for Mapping and Monitoring of Alien Invasive Plant Species (AIPs)." *Physics and Chemistry of the Earth* 112: 237–245. https://doi.org/10.1016/j.pce.2018.12.004.

Sampaio, A. B., and I. B. Schmidt. 2014. "Espécies exóticas invasoras em unidades de conservação federais do Brasil." *Biodiversidade Brasileira* 2: 32–49. https://ecocidio.com.br/wp-content/uploads/2023/05/Especies-Exoticas-Invasoras-em-Unidades-de-Conservacao-Federais-do-Brasil-2.pdf.

Simões, R., G. Camara, G. Queiroz, et al. 2021. "Satellite Image Time Series Analysis for Big Earth Observation Data." *Remote Sensing* 13, no. 13: 2428. https://doi.org/10.3390/rs13132428.

Singh, K. K., T. D. Surasinghe, and A. E. Frazier. 2024. "Systematic Review and Best Practices for Drone Remote Sensing of Invasive Plants." *Methods in Ecology and Evolution* 15, no. 6: 998–1015. https://doi.org/10.1111/2041-210X.14330.

Somodi, I., A. Čarni, D. Ribeiro, and T. Podobnikar. 2012. "Recognition of the Invasive Species *Robinia pseudacacia* From Combined Remote Sensing and GIS Sources." *Biological Conservation* 150, no. 1: 59–67. https://doi.org/10.1016/j.biocon.2012.02.014.

Soto, I., P. Balzani, L. Carneiro, et al. 2024. "Taming the Terminological Tempest in Invasion Science." *Biological Reviews* 99, no. 4: 1357–1390. https://doi.org/10.1111/brv.13071.

Tang, W., G. Long, L. Liu, T. Zhou, M. Blumenstein, and J. Jiang. 2022. "Omni-Scale CNNs: A Simple and Effective Kernel Size Configuration for Time Series Classification." Proceedings of the 10th International Conference on Learning Representations (ICLR 2022). https://arxiv.org/abs/2002.10061.

Taylor, J. E., and J. A. Thomson. 1990. "Allelopathic Activity of Frond Run-Off From *Pteridium esculentum*." In *Bracken Biology and Management*, edited by J. Thomson and R. Smith (No. 40 in Occasional Publication), 203–208. AIAS.

Tian, J., L. Wang, D. Yin, et al. 2020. "Development of Spectral-Phenological Features for Deep Learning to Understand *Spartina alterniflora* Invasion." *Remote Sensing of Environment* 242: 111745. https://doi.org/10.1016/j.rse.2020.111745.

Tongma, S., K. Kobayashi, and K. Usui. 2001. "Allelopathic Activity of Mexican Sunflower [*Tithonia diversifolia* (Hemsl.) A. Gray] in Soil Under Natural Field Conditions and Different Moisture Conditions." *Weed Biology and Management* 1, no. 2: 115–119. https://doi.org/10.1046/j.1445-6664.2001.00020.x.

Turbelin, A., and J. A. Catford. 2021. "Invasive Plants and Climate Change." In *Climate Change*, 515–539. Elsevier. https://doi.org/10.1016/B978-0-12-821575-3.00025-6.

Tuyizere, J., L. Kayitete, P. M. Uhawenimana, et al. 2018. "Mapping of Distribution of Invasive Species in Ruhande Arboretum." *2018 EAJST Special* 8: 15–27.

Valavi, R., J. Elith, J. J. Lahoz-Monfort, and G. Guillera-Arroita. 2019. "blockCV: An R Package for Generating Spatially or Environmentally Separated Folds for k-Fold Cross-Validation of Species Distribution Models." *Methods in Ecology and Evolution* 10, no. 2: 225–232. https://doi.org/10.1111/2041-210X.13107.

Vaswani, A., N. Shazeer, N. Parmar, et al. 2017. "Attention Is All You Need." In *Advances in Neural Information Processing Systems 30 (NIPS 2017)*, 6000–6010. Curran Associates, Inc. https://proceedings.neurips.cc/paper/2017/file/3f5ee243547dee91fbd053c1c4a845aa-Paper.pdf.

Vaz, A. S., D. Alcaraz-Segura, J. C. Campos, J. R. Vicente, and J. P. Honrado. 2018. "Managing Plant Invasions Through the Lens of Remote Sensing: A Review of Progress and the Way Forward." *Science of the Total Environment* 642: 1328–1339. https://doi.org/10.1016/j.scitotenv.2018.06.134.

Villalobos Perna, P., M. Di Febbraro, M. L. Carranza, F. Marzialetti, and M. Innangi. 2023. "Remote Sensing and Invasive Plants in Coastal Ecosystems: What We Know So Far and Future Prospects." *Land* 12, no. 2: 341. https://doi.org/10.3390/land12020341.

Wang, D., W. Cao, F. Zhang, Z. Li, S. Xu, and X. Wu. 2022. "A Review of Deep Learning in Multiscale Agricultural Sensing." *Remote Sensing* 14, no. 3: 559. https://doi.org/10.3390/rs14030559.

Wang, Z., W. Yan, and T. Oates. 2017. "Time Series Classification From Scratch With Deep Neural Networks: A Strong Baseline." 2017 International Joint Conference on Neural Networks (IJCNN), 1578–1585. https://doi.org/10.1109/IJCNN.2017.7966039.

Xu, H., Q. Liu, S. Wang, G. Yang, and S. Xue. 2022. "A Global Meta-Analysis of the Impacts of Exotic Plant Species Invasion on Plant Diversity and Soil Properties." *Science of the Total Environment* 810: 152286. https://doi.org/10.1016/j.scitotenv.2021.152286.

Zaka, M. M., and A. Samat. 2024. "Advances in Remote Sensing and Machine Learning Methods for Invasive Plants Study: A Comprehensive Review." *Remote Sensing* 16, no. 20: 3781. https://doi.org/10.3390/rs16203781.

Zerveas, G., S. Jayaraman, D. Patel, A. Bhamidipaty, and C. Eickhoff. 2021. "A Transformer-Based Framework for Multivariate Time Series Representation Learning." Proceedings of the 27th ACM SIGKDD Conference on Knowledge Discovery & Data Mining, 2114–2124. https://doi.org/10.1145/3447548.3467401.

Zhong, L., L. Hu, and H. Zhou. 2019. "Deep Learning Based Multi-Temporal Crop Classification." *Remote Sensing of Environment* 221: 430–443. https://doi.org/10.1016/j.rse.2018.11.032.

Zhu, E., A. Samat, E. Li, R. Xu, W. Li, and W. Li. 2025. "Adversarial Positive-Unlabeled Learning-Based Invasive Plant Detection in Alpine Wetland Using Jilin-1 and Sentinel-2 Imageries." *Remote Sensing* 17, no. 6: 1041. https://doi.org/10.3390/rs17061041.

Supporting Information

Additional supporting information can be found online in the Supporting Information section. **Figure S1:** Spatial distribution of sampling points across the five stratified spatial folds used for cross-validation. **Figure S2:** Class distribution (number of samples) across the five spatial folds.